

ACCEPTED MANUSCRIPT • OPEN ACCESS

Spin-polarized electron transmission through chiral halocamphor molecules

To cite this article before publication: Joan M. Dreiling *et al* 2018 *J. Phys. B: At. Mol. Opt. Phys.* in press <https://doi.org/10.1088/1361-6455/aae1bd>

Manuscript version: Accepted Manuscript

Accepted Manuscript is “the version of the article accepted for publication including all changes made as a result of the peer review process, and which may also include the addition to the article by IOP Publishing of a header, an article ID, a cover sheet and/or an ‘Accepted Manuscript’ watermark, but excluding any other editing, typesetting or other changes made by IOP Publishing and/or its licensors”

This Accepted Manuscript is © 2018 IOP Publishing Ltd.

As the Version of Record of this article is going to be / has been published on a gold open access basis under a CC BY 3.0 licence, this Accepted Manuscript is available for reuse under a CC BY 3.0 licence immediately.

Everyone is permitted to use all or part of the original content in this article, provided that they adhere to all the terms of the licence <https://creativecommons.org/licenses/by/3.0>

Although reasonable endeavours have been taken to obtain all necessary permissions from third parties to include their copyrighted content within this article, their full citation and copyright line may not be present in this Accepted Manuscript version. Before using any content from this article, please refer to the Version of Record on IOPscience once published for full citation and copyright details, as permissions may be required. All third party content is fully copyright protected and is not published on a gold open access basis under a CC BY licence, unless that is specifically stated in the figure caption in the Version of Record.

View the [article online](#) for updates and enhancements.

Spin-polarized electron transmission through chiral halocamphor molecules

J.M. Dreiling^{1*}, F.W. Lewis², and T.J. Gay¹

¹ Jorgensen Hall, University of Nebraska, Lincoln, Nebraska 68588-0299, USA

² Department of Applied Sciences, Faculty of Health and Life Sciences, Northumbria University, Newcastle upon Tyne, NE1 8ST, UK

*Correspondence to jmdreiling2@gmail.com. Current address: Honeywell International, Broomfield, Colorado 80021, USA

Abstract: We have measured electron-circularly-dichroic asymmetries when longitudinally-polarized (chiral) electrons are scattered quasi-elastically by chiral halocamphor molecules: 3-bromocamphor ($C_{10}H_{15}BrO$), 3-iodocamphor ($C_{10}H_{15}IO$), and 10-iodocamphor. The proposed dynamic origins of these asymmetries are considered in terms of three classical models related to Mott scattering, target electron helicity density, and spin-other-orbit interactions. The asymmetries observed for 3-bromocamphor and 3-iodocamphor scale roughly as Z^2 , where Z is the nuclear charge of the heaviest atom in the target molecule, but the scaling is violated by 10-iodocamphor, which has a smaller asymmetry than that for 3-iodocamphor. This is in contrast to the asymmetries in the collision channel associated with dissociative electron attachment, in which 10-iodocamphor has a much larger asymmetry. All of the available electron-circularly-dichroic data taken to date are considered in an effort to systematically address the dynamical cause of the observed chiral asymmetries.

1
2
3 When longitudinally-polarized electrons scatter from gas-phase chiral molecules, the scattering
4 cross section for a given collision channel will generally depend on the chirality of both collision
5 partners. This was first demonstrated more than two decades ago with targets of Yb(hfc)_3 for the
6 quasi-total scattering cross section measured by the beam-attenuation, or “transmission” method
7 [1]. These studies were subsequently extended to a variety of other molecules; all non-zero
8 chiral effects measured to date have involved molecules containing at least one atom with a
9 relatively high atomic number (≥ 35) [2,3]. Recently, similar “electron dichroic” effects were
10 seen in electron-induced dissociative reactions (“dissociative electron attachment” or DEA) in 3-
11 bromocamphor and 3- and 10-iodocamphor [4,5]. In all these experiments, the chiral sensitivity
12 of a given reaction channel is characterized by an asymmetry parameter a :

$$a_{+(-)} = (I_{\uparrow} - I_{\downarrow}) / (I_{\uparrow} + I_{\downarrow})_{+(-)}, \quad (1)$$

13
14
15
16
17
18
19
20
21
22
23
24
25
26
27
28
29
30 where I corresponds to the detected current for a given scattering channel with spin-forward (\uparrow)
31 or spin-backward (\downarrow) incident electrons. The “+” and “-” subscripts refer to the handedness of
32 the chiral target. Experiments with gas-phase chiral targets have an advantage over those with
33 fixed targets in that any measured non-zero value of a constitutes a clean signature of the effect
34 of target chirality in the scattering process; fixed-target experiments can exhibit similar effects
35 due solely to chiral collision geometry. The disadvantage of random target orientation is that the
36 values of a are generally quite small, rarely exceeding 2×10^{-4} . An interesting exception to this
37 is the case of 3-iodocamphor in the DEA channel, for which a is about an order of magnitude
38 larger [5].

39
40
41
42
43
44
45
46
47
48
49
50
51
52 While the chiral symmetry of these experiments permits a to be non-zero, it provides no
53 clues as to the dynamical mechanisms that might produce such electron-dichroic effects. The
54
55
56
57
58
59
60

1
2
3 studies mentioned above have generally been designed to answer this question by varying either
4 the molecular target's Z - the atomic number of the molecule's heaviest atom - or the target's
5 stereochemical structure, or both. These efforts have largely failed to provide unambiguous
6 evidence of a specific, generally applicable mechanism of chiral selectivity [5-7]. Moreover, no
7 broad theoretical effort has yet been mounted to shed light on this problem. The experiments
8 reported here, measurements of transmission asymmetries with 3-bromocamphor and 3- and 10-
9 iodocamphor, provide new information relevant to some aspects of chirally-sensitive scattering,
10 but they also fail to identify a single, overarching dynamical scattering model that explains the
11 asymmetries we observe. Nonetheless, they do permit us to make the most comprehensive
12 assessment to date of chiral collision dynamics in electron-molecular collisions.

13
14
15
16
17
18
19
20
21
22
23
24
25
26
27 Three qualitatively different mechanisms have been proposed in the literature to account
28 for electron circular dichroism in both transmission and in DEA. We refer to them as
29 "Mott/plural scattering", "spin-other-orbit coupling", and "helicity-density" dynamics (see figure
30 1). They are discussed here specifically for transmission measurements in terms of simple
31 classical pictures that explain why one direction of longitudinal electron spin is more likely to be
32 scattered than the other [6-12]. (Similar classical pictures that pertain to DEA have been
33 described elsewhere [5].)

34
35
36
37
38
39
40
41
42
43
44 In Mott/plural scattering [9], an incident electron is first Coulombically scattered away
45 from the forward direction by a relatively light atom in the target (figure 1 (a)), changing the
46 electron's momentum without significantly affecting its spin. Subsequent large-angle Mott
47 scattering from the high- Z atom in the molecule has a preferential direction that depends on the
48 incident electron's spin. This in turn can result in enhanced scattering back into the forward
49 direction for, e.g., spin-forward electrons. In figure 1(a), the chirality of the molecule is such
50
51
52
53
54
55
56
57
58
59
60

1
2
3 that the lower atom, which could rescatter the electron with “backward” spin, is missing on
4 average (illustrated as the crossed-out atom). While such an effect can also occur with an
5 oriented achiral target, it would average to zero over all molecular orientations. Mott
6
7 asymmetries of the type discussed here scale as Z^2 [13].
8
9
10
11

12
13 Spin-other-orbit interactions (figure 1(b)) occur due to current in the target molecule
14 driven by the Coulombic impulse of an approaching electron [10, 11]. Thinking of a chiral
15 molecule as a conducting helix, it is apparent that such a current will produce both electric and
16 magnetic dipole moments that can act back on the approaching electron. The spin of the incident
17 electron will interact with the magnetic moment produced by the induced orbital angular
18 momentum of the target electrons (the “spin-other-orbit” coupling), leading to differences in
19 scattering that depend on the electron’s helicity. Interference between such induced electric and
20 magnetic dipoles is responsible for optical activity in chiral samples [12]. This effect does not
21 require the presence of a heavy atom in the molecule, but instead relies primarily on the
22 molecular polarizability, which is more closely related to the molecular mass than Z . Thus if
23 spin-other-orbit coupling is the primary mechanism for electron dichroic effects, one might
24 expect there to be a correlation between a and the molecule’s optical rotatory power (ORP), a
25 quantification of a molecule’s optical activity determined by measuring the angle of rotation that
26 the electric field vector of linearly-polarized light experiences while passing through a chiral
27 solution.
28
29
30
31
32
33
34
35
36
37
38
39
40
41
42
43
44
45
46

47
48 Finally, the spin-orbit interaction between a high- Z nucleus and the electrons in a chiral
49 molecule will generally lead to a non-zero expectation value of the “helicity density” operator,
50 $\langle \boldsymbol{\sigma} \cdot \mathbf{v} \rangle$, for the electrons inside the molecule [6, 14, 15]. Here, $\boldsymbol{\sigma}$ and \mathbf{v} are the electron spin and
51 velocity vectors, respectively. This is true even though $\langle \boldsymbol{\sigma} \rangle = 0$ and $\langle \mathbf{v} \rangle = 0$; the chirality of the
52
53
54
55
56
57
58
59
60

1
2
3 target's stereochemistry manifests itself in the chirality of the target electrons. If a target electron
4 is headed in a particular direction within the chiral molecule, its spin will have a non-zero
5 average projection along that direction as well. Helicity density can affect electron scattering if a
6 dynamical difference exists between the scattering of an incident electron by target electrons that
7 have velocity components of opposite sign along the beam direction (figure 1(c)). Assume, for
8 example, that only electrons with velocity components anti-parallel to the beam direction act to
9 scatter incoming electrons to an appreciable angle, and that the target handedness is such that
10 these electrons tend to have a component of spin parallel (as opposed to anti-parallel) to that
11 direction. There would thus be a different cross section for the scattering of one incident
12 electron helicity over the other because of the differences in the singlet vs. the triplet cross
13 sections. Since the helicity density is produced primarily by the spin-orbit interaction of target
14 electrons with the heaviest target nucleus, these effects should also scale as Z^2 [14].
15
16
17
18
19
20
21
22
23
24
25
26
27
28
29
30

31 In the transmission experiments reported here, the targets are variants of camphor in
32 which one hydrogen atom is replaced with either a bromine ($Z = 35$) or iodine ($Z = 53$) atom.
33 These molecules were chosen because they have a reasonably high vapor pressure, they contain a
34 high- Z atom, and we were able to either purchase or synthesize them in both enantiomeric forms.
35 In the case of iodocamphor (see figure 2), the iodine was either attached at a position
36 immediately adjacent to one of the molecule's chiral centers (3-iodocamphor, which we refer to
37 as "3I"), giving a structure equivalent to 3-bromocamphor ("3Br"), or at a position separated
38 from another chiral center by two serial bond lengths (10-iodocamphor, "10I").
39
40
41
42
43
44
45
46
47
48
49
50

51 In our previous measurements of DEA (as opposed to transmission) asymmetries with
52 3Br and 3I [4, 5], a scaled almost perfectly with Z^2 . We were thus surprised when 10I, which we
53 would have expected in a Mott/plural scattering picture to have significantly lower a , exhibited
54
55
56
57
58
59
60

1
2
3 instead the largest value of a observed to date ($> 10^{-3}$). Our subsequent calculations of helicity
4 density for 10I indicated much-reduced values compared with those for 3I. There was also no
5
6 obvious correlation in our DEA data with the ORP of these compounds, apparently ruling out a
7
8 spin-other-orbit mechanism. Thus, the chiral interaction mechanism(s) responsible for
9
10 asymmetries in DEA could not be identified. The measurements of chiral asymmetry in
11
12 transmission reported here were undertaken to clarify the role that the three mechanisms might
13
14 play in a different interaction channel.
15
16
17
18
19

20 The apparatus used for these measurements has been discussed elsewhere [4, 16], so only
21 the most relevant details will be included here. Longitudinally-spin-polarized electrons were
22 photoemitted from a GaAs photocathode [17], with the spin direction determined by the circular
23 polarization of the incident light. The energy width of the electron beam was ~ 0.5 eV, and its
24 polarization was typically $\sim 30\%$ as measured by an optical polarimeter [18]. To reduce
25 instrumental asymmetries, we made use of the feedback system described in reference [19]
26 which combined a spatial filter and quarter-wave plate in the optical setup used for
27 photoemission. The incident electron beam entered the target cell (depicted in figure 3) with the
28 collision energy determined by the voltage applied to the inner target cell. The target cell was
29 kept at ~ 100 °C to prevent target molecules from condensing on the electron-optic elements.
30
31 Inside the target cell, the electron beam was scattered by a chirally-pure molecular target vapor
32 through various interaction channels including, but not limited to, DEA, quasi-elastic scattering,
33 and vibrational excitation. The voltages applied to the retarding meshes following the target cell
34 (elements 6 and 7 in figure 3) were set to discriminate against electrons that had lost energy in
35 collisions with target molecules, and therefore only the quasi-elastically-scattered electrons were
36 allowed to pass out of the target cell and be collected in the Faraday cup.
37
38
39
40
41
42
43
44
45
46
47
48
49
50
51
52
53
54
55
56
57
58
59
60

To perform an asymmetry measurement, molecules of a given handedness were admitted to the target cell until the transmitted electron beam current was reduced to ~30% of its unattenuated value. The “transmission” asymmetry (equation (1)) for these experiments was determined with I being the Faraday cup current (designated as I_t in figure 3). A final asymmetry value, A , was calculated using

$$A = a_- - a_+ = [(I_{\uparrow} - I_{\downarrow})/(I_{\uparrow} + I_{\downarrow})]_- - [(I_{\uparrow} - I_{\downarrow})/(I_{\uparrow} + I_{\downarrow})]_+ \quad (2)$$

At each energy, A was measured ~10 times, and an average was found after applying Chauvenet’s criteria [20] to the data. Statistical uncertainties are given by the standard deviation of the sample mean. By collecting data with two different settings of the quarter-wave plate that circularly polarized the light used to photoemit the electron beam [19], an overall phase shift was introduced into the experiment, and the sign of the measured asymmetry was therefore reversed. The systematic uncertainty was taken to be the absolute value of the sum of the measurements obtained with opposite quarter-wave plate settings. When data was taken with only one of the settings of the quarter-wave plate (as is the case for most of the 3Br data), only the statistical uncertainty is reported. When data was collected at both quarter-wave plate settings, the uncertainty was obtained by combining the statistical and systematic uncertainties in quadrature.

Our transmission data for 3Br, 3I, and 10I are shown in figure 4. (In the following discussion, all values of A will be given in units of 10^{-4} .) The differences between these data and those for DEA with the same targets [5] are striking. The values of A for 3Br in transmission have a maximum magnitude of ~0.7; those in DEA approach 4. In contrast with our DEA experiments, the A -values for the 10I targets in transmission are generally smaller than those for 3I. We assign the largest value for 3I to be 1.1(6) by taking the error-weighted average of the

1
2
3 magnitude of the data at 1.0 and 1.4 eV, whereas for 10I, we measure values of A that are
4
5 consistent with zero. In contrast, the maximum A values in DEA for 3I and 10I are about 8 and
6
7 16, respectively!
8
9

10
11 The current status of all electron-circular-dichroic measurements that have been made to
12
13 date in both transmission and DEA [1-5, 8, 16] are summarized in figures 5-7. In order to assess
14
15 the validity of the three mechanisms discussed above, we have plotted A values both as a
16
17 function of Z^2 and the ORP of the target. If the chiral scattering mechanism is best described by
18
19 Mott/plural scattering or a helicity density picture, A should scale linearly with Z^2 . Given the
20
21 close connection between the spin-other-orbit picture of electron scattering and the
22
23 magnetic/electric dipole interference responsible for optical activity, a clear correlation between
24
25 A and the ORP would support a spin-other-orbit picture. The ORP values for all compounds
26
27 were obtained from the Sigma-Aldrich website [21], with the exception of 3I and 10I, which
28
29 were determined from references [22] and [23], respectively. All ORPs were measured using
30
31 sodium D light ($\lambda = 589$ nm).
32
33
34
35
36

37
38 Figures 5-7 categorize data for three classes of molecular targets: camphor and some of
39
40 its halocamphor and dihalocamphor derivatives, halomethylbutanes, and a class of rare-earth
41
42 (lanthanide) NMR shift reagents in which three camphor-like-ligands (3-
43
44 (heptafluoropropylhydroxymethylene)camphorate (hfc)) surround the rare-earth atom. The
45
46 Münster group [1-3] has taken all of the halomethylbutane, the rare-earth hfc, and the
47
48 dibromocamphor data, exclusively in transmission. Both the Münster group and our group have
49
50 taken transmission data for camphor [1, 8] and 3Br [2, 16], with the results being in good
51
52 agreement. Our group has taken the DEA halocamphor data [4, 5] and the transmission data for
53
54 3I and 10I presented here. It should be emphasized that the experimental parameters for our
55
56
57
58
59
60

1
2
3 transmission studies were different from those of the Münster group. Specifically, they used an
4 electron beam of energy width ~ 0.3 eV and polarization of $\sim 40\%$, and the electron beam was
5 attenuated by $\sim 90\%$ due to target scattering. To make a valid comparison between our data and
6 theirs in figures 5(a) and 5(b), we scaled their bromocamphor and dibromocamphor data to match
7 our experimental conditions as discussed in reference [16]. The Münster halomethylbutane and
8 rare-earth hfc data (figures 6 and 7) are taken directly from the values they reported without any
9 energy convolution or adjustment for incident electron polarization or electron beam attenuation
10 factors.
11
12
13
14
15
16
17
18
19
20
21

22 The data used to create figures 5-7 are the largest reported absolute values of A for a
23 given collision channel and target for incident electron energies > 1 eV. In some compounds, A
24 increases rapidly at the lowest energies investigated. However, as discussed in reference [2] and
25 based upon our own experience, these lowest-energy data are likely contaminated by
26 instrumental effects, and they are therefore not included. This way of presenting the data ignores
27 an important aspect of the electron-molecule chiral interaction: its energy dependence and the
28 probable importance of negative ion resonances. By focusing on the largest value of A for a
29 given target and reaction channel, though, we are presumably selecting the case of optimal
30 collision conditions for chiral interactions and can focus on the zeroth-order problem - possible
31 correlations of A with Z^2 and/or the target's ORP.
32
33
34
35
36
37
38
39
40
41
42
43
44
45

46 The following conclusions may be drawn from the data.
47
48

49 Camphor-derivatives (figure 5). We consider first only the molecules in which the high- Z atom
50 is varied exclusively in the 3-position: camphor, 3Br, and 3I. Both the transmission (figure 5(a))
51 and DEA (figure 5(c)) data scale linearly with Z^2 , but this does not allow us to distinguish
52
53
54
55
56
57
58
59
60

1
2
3 between the helicity density and Mott/plural scattering mechanisms. Much is learned, however,
4 by adding the 10-iodocamphor and the 3,9-dibromocamphor results. The 10I DEA data (figure
5 5(c)) cannot be explained in either a simple Mott scattering picture or by a helicity density
6 calculation [5]. However, in transmission, the helicity density model does account for the
7 reduction of A for both dibromocamphor [6] and 10I [5]. We thus argue that while the
8 transmission data is consistent with Mott/plural scattering, it has more comprehensive,
9 quantitative theoretical support from helicity density calculations [5]. Unfortunately, this view is
10 blurred by the fact that all of the transmission data exhibit a smooth, monotonic (albeit nonlinear)
11 increase of A with ORP (figure 5(b)). The ORP scaling is non-existent for DEA (figure 5(d)).
12 Halomethylbutane derivatives (figure 6). The transmission data scale linearly with both Z^2 and
13 the ORP, so no conclusions can be drawn.
14 Rare-earth complexes (figure 7). Unlike the halomethylbutanes, where A correlates nominally
15 with both ORP and Z^2 , there is no obvious scaling of any kind with the rare-earth hfc's. We note
16 that while the ORP values are positive for three of the targets, the largest A occurs for Yb(hfc),
17 which actually has a negative ORP.

18
19
20
21
22
23
24
25
26
27
28
29
30
31
32
33
34
35
36
37
38
39 The camphor-family transmission data, shown in figures 5(a) and 5(b), have provided the
40 most complete picture to date of how a chiral stereochemical system scatters polarized electrons.
41 Like the DEA 3Br and 3I data, the transmission data scale well with Z^2 , but with transmission,
42 the 10I and dibromocamphor data departures from this simple scaling can be explained semi-
43 quantitatively by helicity density calculations [5,6] and, in a more hand-waving way, by a Mott
44 scattering picture. This would seem to give a first, incremental understanding of the electron-
45 chiral molecule scattering problem, were it not for the fact that the transmission A -values for the
46 entire camphor family lie on a fairly smooth, monotonically-increasing curve that is a function of
47
48
49
50
51
52
53
54
55
56
57
58
59
60

1
2
3 the ORP of the target. Overall, these emergent patterns of functional dependence still don't
4 allow us to identify unambiguously a dynamical scattering model for these targets. It is at least
5 clear that DEA and quasi-elastic total scattering rely differently upon the (crudely-characterized)
6 classical mechanisms we have identified here.
7
8
9
10
11
12

13 It would be interesting to revisit the rare-earth hfc targets, which are “propeller”
14 molecules, having the high-Z rare earth atom at the hub of the three camphorate-ligand (hfc)
15 “blades.” The Münster data were taken with targets in which all the blades had the same
16 camphor-like chirality, but which were racemic mixtures of left- and right-handed blade
17 configurations. Thus, the heavy atom was not at a chiral center of the molecule. New
18 experiments with targets having chirally-pure blade arrangements might yield a correlation of A
19 with either Z^2 or ORP. More generally, the future of these studies must surely include a more
20 robust theory effort.
21
22
23
24
25
26
27
28
29
30

31 32 **ACKNOWLEDGEMENTS** 33

34
35 The authors would like to thank P.D. Burrow for his substantial assistance throughout this
36 project. This work was funded by the U.S. National Science Foundation, Grant Nos. PHY-
37 1206067 and PHY-1505794. We also thank Northumbria University for awarding an
38 Anniversary Research Fellowship to FWL.
39
40
41
42
43
44
45
46
47
48
49
50
51
52
53
54
55
56
57
58
59
60

REFERENCES

- [1] Mayer S and Kessler J 1995 *Phys. Rev. Lett.* **74** 4803
- [2] Mayer S, Nolting C and Kessler J 1996 *J. Phys. B: At. Mol. Opt. Phys.* **29** 3497
- [3] Nolting C, Mayer S and Kessler J 1997 *J. Phys. B: At. Mol. Opt. Phys.* **30** 5491
- [4] Dreiling J M and Gay T J 2014 *Phys. Rev. Lett.* **113** 118103
- [5] Dreiling J M, Lewis F W, Mills J D and Gay T J 2016 *Phys. Rev. Lett.* **116** 093201
- [6] Scheer A M, Gallup G A and Gay T J 2006 *J. Phys. B: At. Mol. Opt. Phys.* **39** 2169
- [7] Gay T J 2009 *Adv. At. Mol. Phys.* **57** 157
- [8] Trantham K W, Johnston M E and Gay T J 1995 *J. Phys. B: At. Mol. Opt. Phys.* **28** 1543
- [9] Kessler J 1982 *J. Phys. B* **15** 101
- [10] Walker D W 1982 *J. Phys. B* **15** 289
- [11] Gallup G A in *Electron Collisions with Molecules, Clusters, and Surfaces*, edited by Ehrhardt H and Morgan L A 1994 (Plenum, New York) pps. 163-170
- [12] Condon E U 1937 *Rev. Mod. Phys.* **9** 444
- [13] Mott N F and Massey H S W 1965 *The Theory of Atomic Collisions*, 3rd ed. (Oxford, New York) p. 235.
- [14] Rich A, Van House J and Hegstrom R A 1982 *Phys. Rev. Lett.* **48** 1341

- 1
2
3 [15] Gay T J, Johnston M E, Trantham K W and Gallup G A 1996 in *Selected Topics in Electron*
4 *Physics*, edited by Campbell D M and Kleinpoppen H (New York, Plenum) pps. 159-170
5
6
7
8 [16] Dreiling J M and Gay T J 2015 *J. Phys.: Conf. Ser.* **635** 012015
9
10
11 [17] Pierce D T, Celotta R J, Wang G -C, Unertl W N, Galejs A, Kuyatt C E and Mielczarek S R
12
13 1980 *Rev. Sci. Instrum.* **51** 478
14
15
16 [18] Gay T J, Furst J E, Trantham K W and Wijayaratna W M K P 1996 *Phys. Rev. A* **53** 1623
17
18
19 [19] Dreiling J M, Burtwistle S M and Gay T J 2015 *Appl. Opt.* **54** 763
20
21
22 [20] Bevington P R and Robinson D K 1992 *Data Reduction and Error Analysis for the Physical*
23 *Sciences* (McGraw Hill, New York) p. 58.
24
25
26 [21] <http://www.sigmaldrich.com/united-states.html>
27
28
29 [22] Mathieu J P and Perrichet J 1935 *Comptes Rendus Hebdomadaires des Seances de*
30 *l'Academie des Sciences* **200** 1583
31
32
33 [23] Lewis F W, Egron G and Grayson D H 2009 *Tetrahedron: Asymmetry* **20** 1531
34
35
36
37
38
39
40
41
42
43
44
45
46
47
48
49
50
51
52
53
54
55
56
57
58
59
60

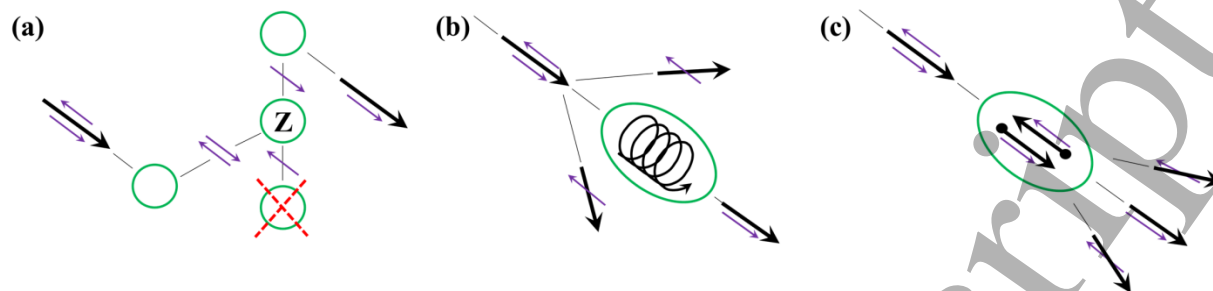


Figure 1. Schematic diagrams of collisional mechanisms in transmission experiments leading to chiral asymmetries showing (a) Mott scattering, (b) spin-other-orbit coupling, and (c) helicity density (see text).

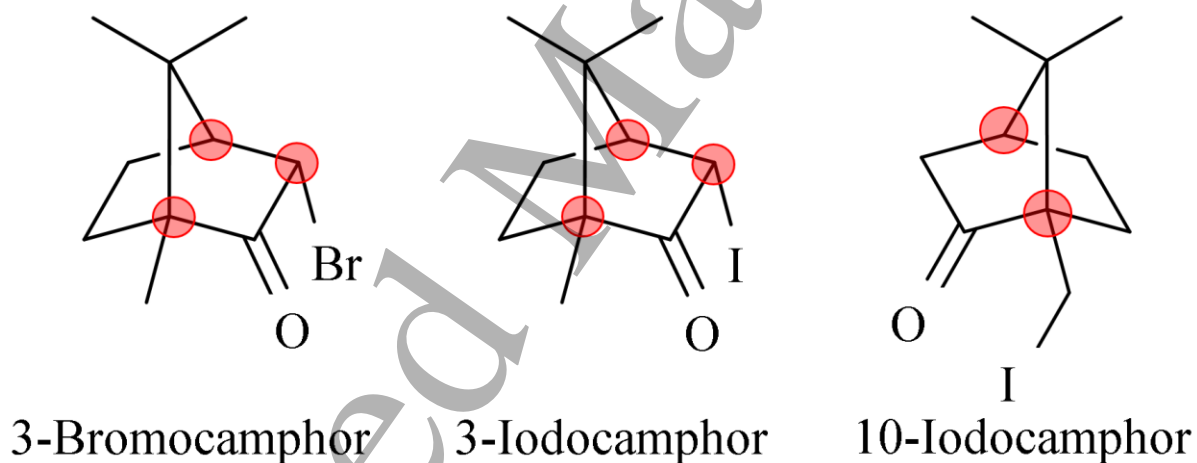


Figure 2. Chiral camphor-derivative molecules studied in this experiment. The (+)-enantiomers are shown, and chiral centers are indicated with red circles.

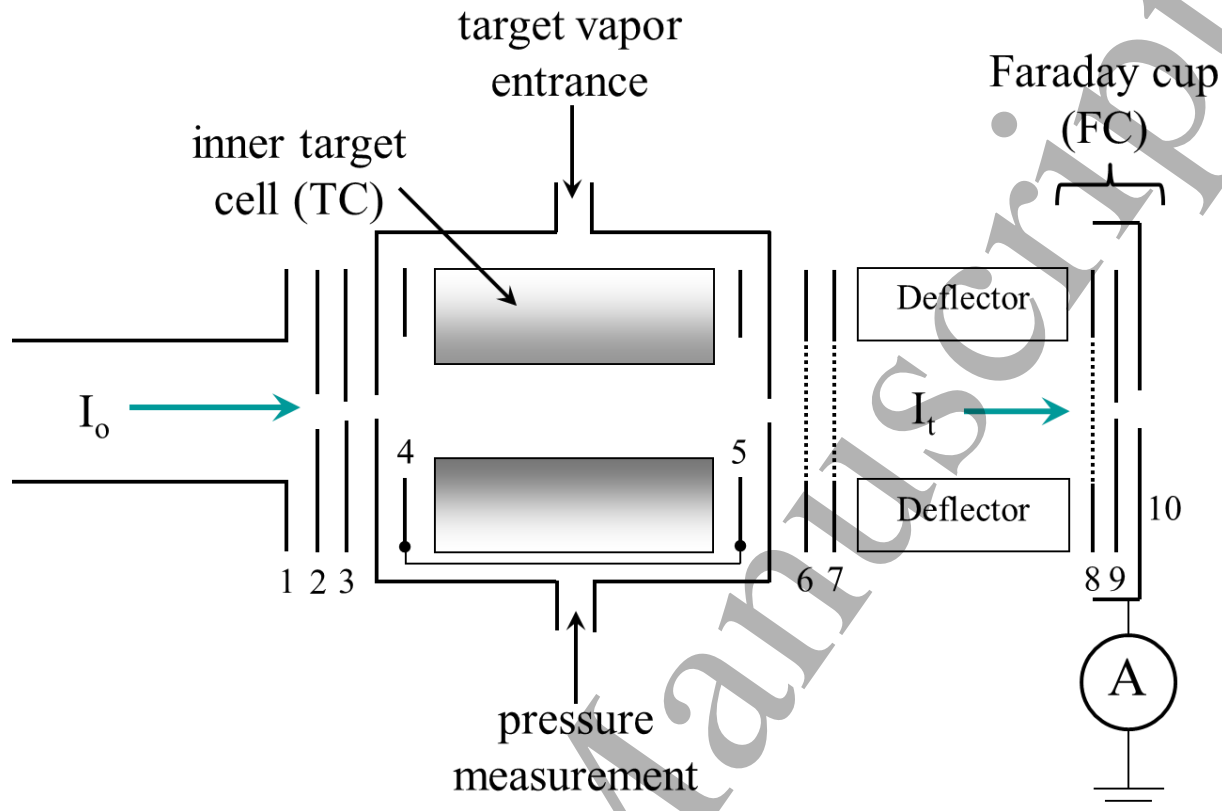


Figure 3. Schematic of the target elements, including the incident (I_o) and transmitted (I_t) electron beams, the target cell structure, and the Faraday cup assembly (elements 8-10) used to measure the transmitted beam. Other electrostatic lens elements (1, 2, 4, 5), retarding-field meshes (6, 7), and a beam-defining aperture (3) are indicated as well. Figure from [4].

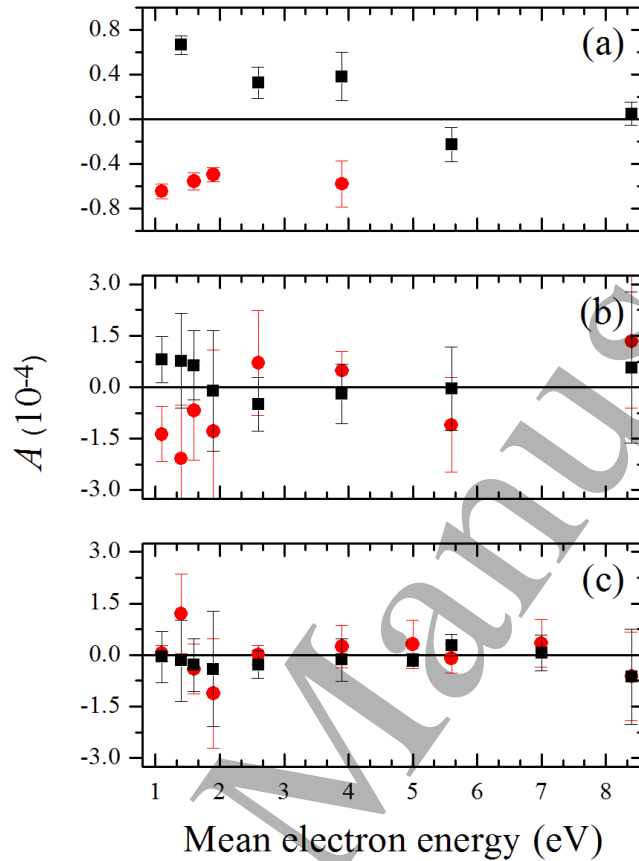


Figure 4. Measured transmission asymmetries, A , as a function of mean electron energy for each halocamphor compound investigated in this study: (a) 3-bromocamphor (3Br), (b) 3-iodocamphor (3I), and (c) 10-iodocamphor (10I). Squares (black) and circles (red) represent opposite settings of the final quarter-wave plate, which should give asymmetry measurements of opposite sign. When asymmetry data was collected at both quarter-wave plate settings, the uncertainty was calculated by finding the quadrature sum of the statistical and systematic uncertainties (see text). For data collected at only one quarter-wave plate setting, the uncertainty is just the statistical uncertainty.

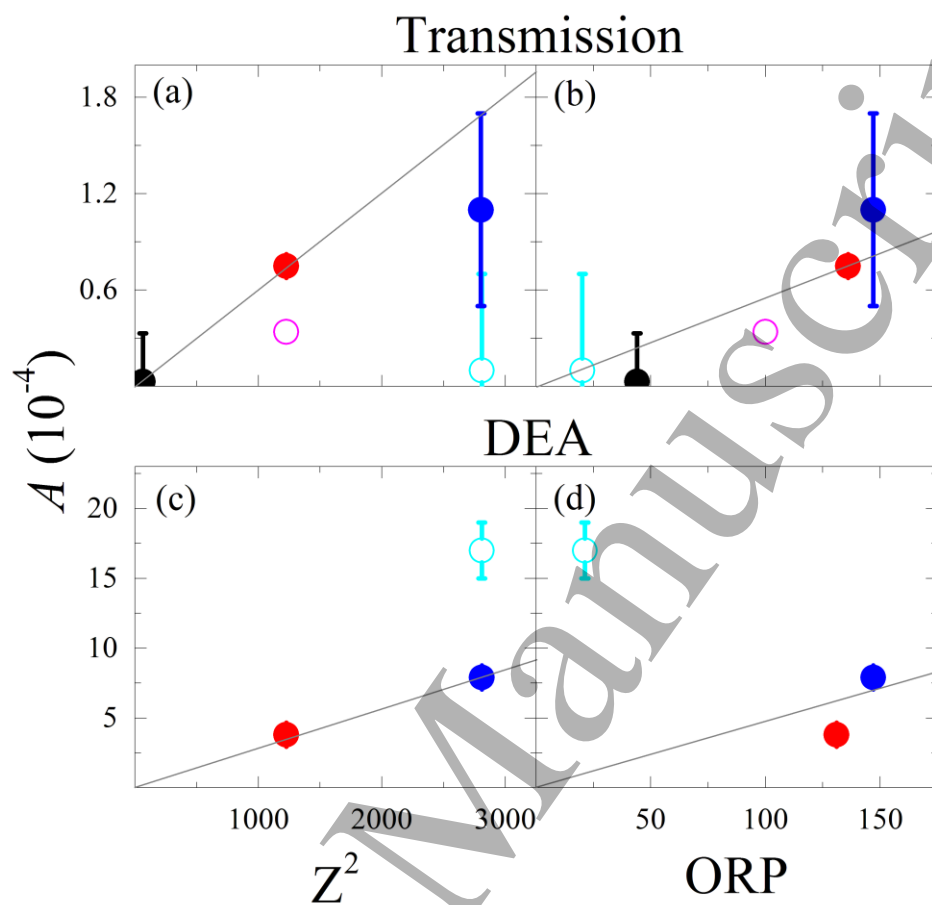


Figure 5. Electron circular dichroism asymmetries, A , with camphor-derivative targets for both quasi-elastic scattering in transmission (a, b) and dissociative electron attachment (DEA; c, d). The data are plotted as a function of the optical rotatory power (ORP) and Z^2 , where Z is the highest nuclear charge in the molecule. Open circles denote either 10-iodocamphor (light blue) or 3,9-dibromocamphor (magenta), and solid circles correspond to camphor (black), 3-bromocamphor (red), and 3-iodocamphor (blue). The solid lines are linear fits to the data forced through zero.

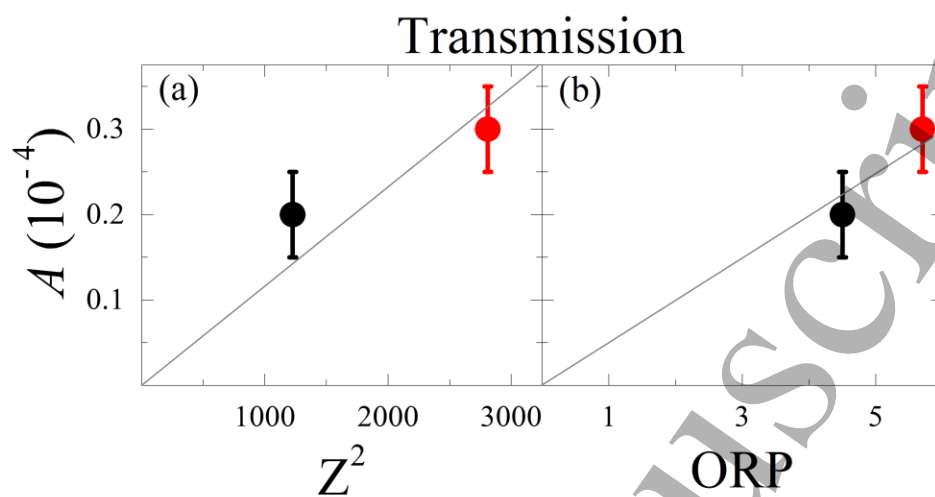


Figure 6. Values of A for the halomethylbutane targets of bromomethylbutane (black) and iodomethylbutane (red).

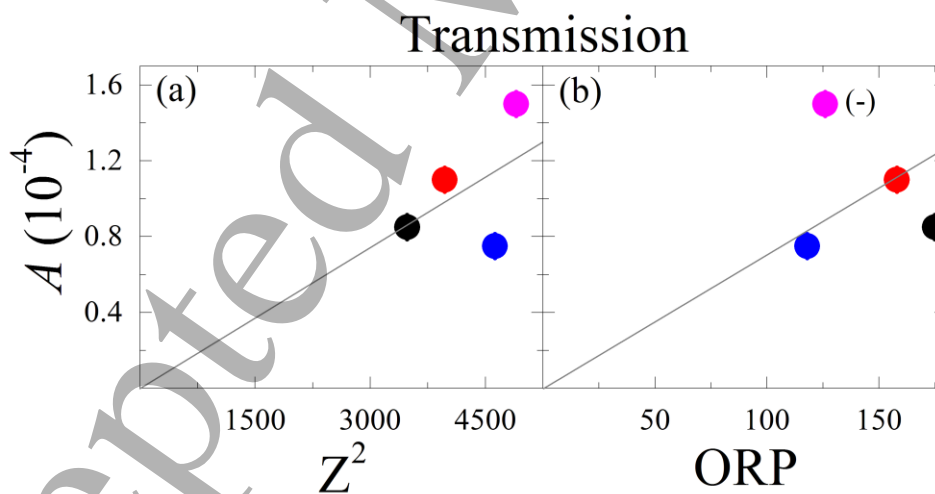


Figure 7. Values of A for the rare-earth targets of $\text{Pr}(\text{hfc})_3$ (black), $\text{Eu}(\text{hfc})_3$ (red), $\text{Er}(\text{hfc})_3$ (blue), and $\text{Yb}(\text{hfc})_3$ (magenta). The (-) indicates that the sign of the ORP for the $\text{Yb}(\text{hfc})_3$ target is opposite that of the others.